 doi:10.20944/preprints202210.0170.v1

Article

Influence of Cellulose Nanofibers on the Behavior of Pickering Emulsions. Part 1. Microscopy and Startup Flow Test

Shu-Ming Cui[1,2], Saud Hashmi[3], Wen-Qiang Li[1], Stephan Handschuh-Wang[4], Cheng-Tian Zhu[1], Shi-Chang Wang[1], Pian-Pian Yang,[5] Yan-Fei Huang[1]*, Guang-Ming Zhu[1]* and Florian J. Stadler[1]*

[1] College of Materials Science and Engineering, Shenzhen Key Laboratory of Polymer Science and Technology, Guangdong Research Center for Interfacial Engineering of Functional Materials, Nanshan District Key Laboratory for Biopolymers and Safety Evaluation, Shenzhen University, Shenzhen 518055, PR China
[2] South China Advanced Institute for Soft Matter Science and Technology, School of Emergent Soft Matter, South China University of Technology, Guangzhou 510640, PR China
[3] Department of Polymer & Petrochemical Engineering NED University of Engineering & Technology Karachi, Sindh 75270, Pakistan
[4] College of Chemistry and Environmental Engineering, Shenzhen University, Shenzhen 518060, People's Republic of China
[5] College of Management, Shenzhen University, Shenzhen 518055, PR China
* YFH: yanfeihuang@szu.edu.cn , ZGM: gmzhu@szu.edu.cn FJS: fjstadler@szu.edu.cn

Abstract: When existing at emulsion interface and continuous phase, dispersibility of water-soluble flexible polymer chains has obvious effect on rheology and dielectric properties of whole emulsion. CNF Pickering emulsion is a good system to research these properties with respect to their microscopic phase structure, dielectric and rheological properties by using cellulose nanofibers (CNF) as water-soluble Pickering emulsifier, liquid Paraffin as oil phase and DDAB as a cationic auxiliary surfactant. The CNF- and DDAB-contents were systematically varied while the water to paraffin oil ratio remained constant to discern the influence of the Pickering emulsifiers. Polarized optical microscopic images revealed that the droplets have tendency to become smaller size for higher CNF content, but bigger size for higher DDAB content, which was proved by the fluorescent analysis for CNF dispersibility with varying DDAB content. The dielectric damping exhibits a minimum, whose value decreases with increasing DDAB- and CNF-content. Increasing the DDAB-content promotes solubilization of CNFs in the aqueous phase and will increase the overall viscosity and yield points. Similarly, a higher CNF-content leads to a higher viscosity and yield point, but at high DDAB-contents the viscosity function exhibits an S-shape at intermediate CNF-content. To evaluate the results further they were compared with CNF-dispersions (without oil-phase), which showed a surfactant effect slightly on maximum stress but strongly on yield stress τ_y, indicating DDAB can promote the formation of CNF network rather than the viscosity of whole system.

Keywords: cellulose nanofibers; CNF networks; physical entanglement; droplets clusters; startup flow

1. Introduction

1.1. Overview of CNF stabilized emulsion systems

An emulsion is a dispersed system composed of an oil and an aqueous phase with an emulsifier (surfactant or Pickering emulsifier) adsorbed at the interface. One of attracted emulsifier: cellulose, the natural, environmental, and renewable material, consists of dehydrated glucose units. These glucose (hexose) units comprise abundant hydroxy and carboxyl moieties as hydrophilic groups and polymer backbone, and are widely applied as biocompatible emulsifiers and thickeners. Nanocellulose refers to ultra-fine cellulose. It is an amphiphilic organic polymer, with a diameter between 1~100 nm. Cellulose nanocrystal (CNC) [1-3], microfibrillated cellulose (MFC) [4-6], bacterial nanocellulose (BNC) [7-10], and cellulose nanofibers (CNF) [11] belong to the class of nanocellulose. In

 doi:10.20944/preprints202210.0170.v1

general, emulsions stabilized with CNF or CNC can behave gel-like because of the strong, irreversible cellulose adsorption at the O/W (oil/water) interface [2], using the steric interfacial stabilization [12]. As rod-like particles, CNC has near-perfect crystallinity (ca. 90%), while CNFs with micrometer-long entanglements contain both amorphous and crystalline domains [12-14]. Therefore, CNFs, particularly, their flexible chains and crystalline domains, contribute to the complex properties at the interface and in the continuous phase. Jiang et al. [15] have reported that an increase in CNF content increases the emulsions' bulk storage and loss modulus, which is related to the dense network formation in the bulk phase. Kalashnikova et al. [16] proved that long cellulose nanocrystals with densely entangled chains can form ultrastable emulsions and interconnected network of low covered droplets (40%), compared with shorter nanocrystals that merely show a densely interfacial absorption rather than the role in connection among each droplets. Li et al. [17] studied different CNC particles fabricated from pure CNFs by hydrolyzation with sulfuric acid-for 1, 2, and 4h. They reported that the viscosity curves of pure CNF emulsions present a remarkable deviation comparing with curve of the mixture of CNF and crystallized at shear rate ramp of 10~100 1/s, which proved the crosslinked feature in aqueous phase affecting from CNF flexible matrixes rather than dense aggregation of rod-like CNC particles. Physical entanglements of CNFs and solid-like viscoelastic properties can be easily created in aqueous phase due to the large aspect ratio and high flexibility of CNFs, even at very low concentrations, and this sets them apart from short and rod-like CNC structures, which necessitate higher concentrations. In addition, CNF emulsions feature a certain shear-thinning behavior [17, 18].

1.2. Enhancement of interfacial adsorption using an auxiliary surfactant

Pickering particles cannot maintain the interfacial force balance merely by intermolecular forces due to weak interfacial interaction associated with balanced contact angle between aqueous and oil phases, possibly resulting in droplet rupture in the course of rapid rheology profiles or long-term storage [19-21]. Hence, surfactants are often employed to overcome this issue. When the surfactant has a strong electrostatic attraction with the Pickering stabilizers and dispersed droplets, it promotes the formation of complex interfaces rather than desorption of the particles [22]. In other words, additional ionic surfactants can establish a bridge between particles and dispersed droplets through stronger ionic adsorption to enhance interfacial stability, which is essential for stabilizing emulsion systems [23]. For instance, Hong et al. [24] studied the effect of addition of CTAB (full name) on the improvement of the interfacial attraction between clays and oil and increase in the interfacial modulus. These effects are strong enough to provide a barrier against droplet coalescence. Similarly, Whitby et al. [25] concluded that the auxiliary surfactant (octadecylamine) is able to affect the aggregate's state of Pickering particles (laponite) in water. Specifically, the surfactant affects the droplets' size and prevent droplets' coalescence in the emulsion by means of the synergistic and antagonistic interaction between laponite and octadecylamine, respectively [21]. In conclusion, the present of auxiliary ionic surfactants improve the interfacial adsorption of stabilizers at the interface by stronger electrostatic connection. If not, interfacial modulus would decreased due to desorption of interfacial localized [24].

It is vital for this article to discuss the distribution of CNF chains at the interface and continuous phase in emulsion systems using changing CNF and auxiliary surfactant content. Polarized optical, electronic, and fluorescence microscopy and steady rheological studies are analyzed to assess the droplet's size, CNF distribution, and bulk flow behavior.

1.3. Dielectric spectroscopy on Pickering emulsion

Broadband dielectric spectroscopy (BDS) can study the structure and stability of emulsions and their response to alternating current (AC) fields, not only for dielectric properties affected by droplets and surfaces, but also abnormal states, such as phase separation, flocculation, and droplet coalescence [26]. BDS uses a frequency generator to

Preprints (www.preprints.org) | NOT PEER-REVIEWED | Posted: 12 October 2022 doi:10.20944/preprints202210.0170.v1

create a sinusoidal electrical signal applied to the samples by perturbing the electrode and arising an alternating current [27]. Then, the relevant parameters about the examined samples, such as permittivity, conductivity, and impedance, can be obtained owing to the movement of charged groups to overcome the stimulus of continuous changing fields [28, 29]. Furthermore, these dielectric parameters characterize many mechanisms, for instance, interfacial polarization, phase balance, and relaxation behavior [30].

When it comes to BDS studies of emulsions and other colloidal systems, Sjöblom et al. and Sen et al. reported that both the permittivity at low and high frequency and relaxation time could be used to obtain information on flocculation in emulsions caused by electric fields [31, 32]. Moreover, permittivity in BDS can monitor the phase separation more effectively compared with conductivity measurements [26]. The BDS study of the emulsion can be equivalent to the form of a resistor with a capacitor in parallel (Boyle model) [33], while a phase separation can be described by serial capacitor analogy. As emulsifiers accumulate at the interface, the conductivity of the emulsifiers is more prominent than that of the interface, irrespective of the capacitances of the interface barrier [34]. However, the emulsion system is only metastable because of the possibility of sedimentation, flocculation, and coalescence of bulk droplets, which will directly influence the impedance and polarization, which characterize the change of emulsion state, droplets stability, and desorption at the interface [26, 35].

1.4. Steady rheological studies on cellulose-based emulsions

There is a broad application for nanocellulose emulsions prepared by using CNC [12], MFC [36-38], BNC, [39, 40] and CNF [41]. Recently, the viscosity enhancement in emulsions upon introduction of nanocellulose as Pickering emulsifiers has been of great interest. These nanocellulose emulsifiers reside at the oil-water (O/W) interface, and are interesting as they are a renewable and nontoxic emulsifiers [42, 43]. CNFs can stabilize emulsions by forming a shell around the droplets, creating a steric barrier, and stabilized emulsions exhibit rigid solid-like viscoelastic properties under low shear forces, even at low CNF contents [16]. This is due to the formation of a highly entangled network and its viscosity increase with a higher CNF content, which also leads to a remarkable shear-thinning behavior [17, 18]. Dickinson et al. [44] proved that those hydrocolloid-coated droplets could be immobilized by the surrounding polymer network and cause gelation, showing the yield behavior if the polymer content increases; oppositely, the whole system could become unstable because of weak connection throughout droplets at low polymer content. However, an excess of stabilizers cannot further promote the emulsion stability, resulting from the possibility of dominating interparticle adsorption or flexible chains entanglements [45, 46].

The viscosity studies of CNF emulsion or dispersions with different auxiliary ionic surfactants or CNF content had similar results as the work of Li et al [17], which is corroborated by optical and confocal laser microscopic and dielectric research for this paper.

2. Materials and Methods

2.1. Materials

Cellulose Nanofibers with a diameter of 5-100 *nm*, crystallinity of 70-90%, and length of >1 *μm*, dispersed in water at a concentration of 4.5 wt.% were obtained from Zhongshan Nano bio-materials co-Ltd (Zhongshan, China). The raw CNF dispersion is diluted to the desired concentration, which use for an entirely aqueous phase for CNF emulsion. Didodecyl-dimethyl-ammonium bromide (DDAB, Aladdin, Shanghai) dissolved in chloroform (Aladdin, Shanghai, China) was used as the secondary emulsifier to enhance the stability of CNF in O/W interface. The oil phase was prepared by mixing 9 parts (by volume) liquid paraffin (Macklin, Shanghai, China) and 1 part chloroform DDAB solution. The compositions of the analyzed CNF emulsion samples are shown in Table 1. The mixed oil phase was added to the aqueous phase until an oil to water ratio of 1:2 was achieved. Then, the separated phases were emulsified by mechanical homogenization at 11,600 rpm

 doi:10.20944/preprints202210.0170.v1

for 3 min using a high-speed homogenizer (IKA T-10, Frankfurt, Germany). Meanwhile, the CNF aqueous dispersion samples with 0, 0.1, 0.3 and 0.5 wt.% DDAB content were prepared for steady rheological analysis. The steady rheological analysis was executed analog to the startup-flow test of the other emulsion samples, which was used to prove the degree of CNF entanglement in the aqueous phase. The appearance of all samples with varying CNF content are shown in Figures SI1 and SI2, which shows the yield stress (some cannot flow down) except for sample of CNF0.5 & 1%-DDAB0.1%. of the degree of dilution with water can be calculated by Eq SI1. The determined values are listed in Table SI1.

Table 1. Composition of analyzed CNF emulsions

Sample	CNF [wt.%]	DDAB [wt.%]	O:W ratio
CNF 0.5%-DDAB 0.1%	0.5		
CNF 1%-DDAB 0.1%	1		
CNF 1.25%-DDAB 0.1%	1.25		
CNF 1.5%-DDAB 0.1%	1.5		
CNF 1.75%-DDAB 0.1%	1.75	0.1	1:2
CNF 2%-DDAB 0.1%	2		
CNF 2.5%-DDAB 0.1%	2.5		
CNF 2.75%-DDAB 0.1%	2.75		
CNF 3%-DDAB 0.1%	3		
CNF 0.5%-DDAB 0.5%	0.5		
CNF 1%-DDAB 0.5%	1		
CNF 1.5%-DDAB 0.5%	1.5	0.5	1:2
CNF 2%-DDAB 0.5%	2		
CNF 2.5%-DDAB 0.5%	2.5		
CNF 3%-DDAB 0.5%	3		
CNF 2.5%-DDAB 0.1%		0.1	
CNF 2.5%-DDAB 0.2%		0.2	
CNF 2.5%-DDAB 0.3%	2.5	0.3	1:2
CNF 2.5%-DDAB 0.4%		0.4	
CNF 2.5%-DDAB 0.5%		0.5	

2.2. Methods

Microscopy. Polarized Optical Microscopy (POM) images of CNF emulsions were investigated by an Axio Scope A1 polarized optical microscope (ZEISS, Scope A1, Germany). Distinct and sparse CNF structures were captured by preserving a diluted CNF solution (ca. 0.8 wt‰) in a negative stain, which can be visualized using transmission electron microscopy (TEM) images (JEOL-2100F, Japan) to evaluate their nanofibers' network and conformational states. Due to the specific fluorescence property of liquid paraffin, the droplets' shapes can be easily observed These droplets shapes were analyzed using Fluorescence Microscopy (Nikon, ECLIPSE Ti2-E, Japan) with the DAPI channel at a wavelength of 460 nm. To gain several clear images of CNF distribution in the water phase, Furthermore, CNF chains were stained with a small amount of Calcofluor white, followed by detection with confocal laser scanning microscopy (ZEISS-LSM880, Germany) in order to study the state of polymer distribution at aqueous phase with different DDAB content. Scanning electron microscopy images (Hitachi SU-70, Japan) of different dried (i.e., water-free) CNF emulsions visualized the structures. Unlike for the other emulsions in this paper, these images were taken using room-temperature solid paraffin, which otherwise is identical in terms of interfacial properties to avoid changes to the morphology. The solid samples were prepared by emulsifying at 80°C and in same rotating speed. Afterwards, the heat emulsion become cool down and totally solid-like, then the remain water was removed by freeze-drying.

Preprints (www.preprints.org) | NOT PEER-REVIEWED | Posted: 12 October 2022 doi:10.20944/preprints202210.0170.v1

Dielectric spectroscopy. The CNF emulsions were measured dielectrically using the BDS (Concept 40, Novocontrol Technologies, Montabaur Montabaur, Germany) by preparing the samples between two same-sized gilded copper electrodes (diameter 20 mm, gap 0.1 mm, set by quartz rods with defined diameter), as shown in Figure SI3. In a dielectric or impedance measurement, a voltage of 1.0 V_{rms} (i.e., root-mean-square voltage) with a frequency (f) is applied to a sample cell. The electrical properties of CNF emulsion are measured at constant room temperature (T=25°C) and frequency sweeps, with an AC electric field of 1.0 V_{rms} and a variable frequency f =10^{-2}…10^{7} Hz, starting at the highest frequency. As the emulsions are deformed during sample loading, it will take a while to reach an equilibrium state for the structure again. For this reason, the abovementioned frequency sweeps are repeated until the equilibrium state has been reached, usually after 1-2 h. In general, 5 frequency sweep cycles (CNF2%-DDAB0.1%) were sufficient to reach an equilibrium response (Figure SI4). Only the data in equilibrium was further evaluated.

Rheology. Rheological experiments were conducted on an Anton Paar MCR 302 (Graz, Austria), equipped with a Peltier heated lower plate and a Peltier hood. This heating system was tightly closed and the air in the oven was saturated with water to minimize sample evaporation. Measurements were carried out at 25 °C using a 50 mm/1° cone and plate geometry (CP50), with a gap (cone truncation) of 102 μm, avoiding bridging successfully. The rheological protocol is startup flow, as for the basic flow behavior, which includes two up and down loops of shear rate ramps ($\dot{\gamma}$=0.01…1000 s^{-1}/1000…0.01 s^{-1} with a logarithmic increase or decrease of $\dot{\gamma}$ and a ramp time of 920s, **Error! Reference source not found.**). While usually, the differences between run 2, 3, and 4 are relatively small, only the data of the last run will be discussed. The resulting viscosity functions $\eta(\dot{\gamma})$ and shear stress functions $\tau(\dot{\gamma})$ as well as the normal force functions $F_n(\dot{\gamma})$ are evaluated with respect to obtaining the yield stress τ_y, the viscosity/stress at high shear rate, and the normal force differences $F_n(\dot{\gamma}$=1000 $s^{-1})$ vs. $F_n(\dot{\gamma}$=0.01 $s^{-1})$.

3. Results

3.1. Morphological observations

Interfacial structure, including CNF chains and DDAB, stabilized the oil phase (liquid paraffin – chloroform mixture). The proposed stabilization mechanism is shown in Figure 1. DDAB, as the auxiliary surfactant, resides at the oil-water interface, and stabilize the emulsion. The positive charge is conducive for the stabilization of the Pickering emulsion with the CNFs, as electrostatic forces between the auxiliary stabilizer and the CNF further stabilize the interfaces. Moreover, DDAB can be present in the system as regular micelles (in the aqueous phase) or as inverse micelles in the oil phase. CNF and DDAB interact with each other through the charged DDAB-head group (N^+) and the O^{2-} of CNF.

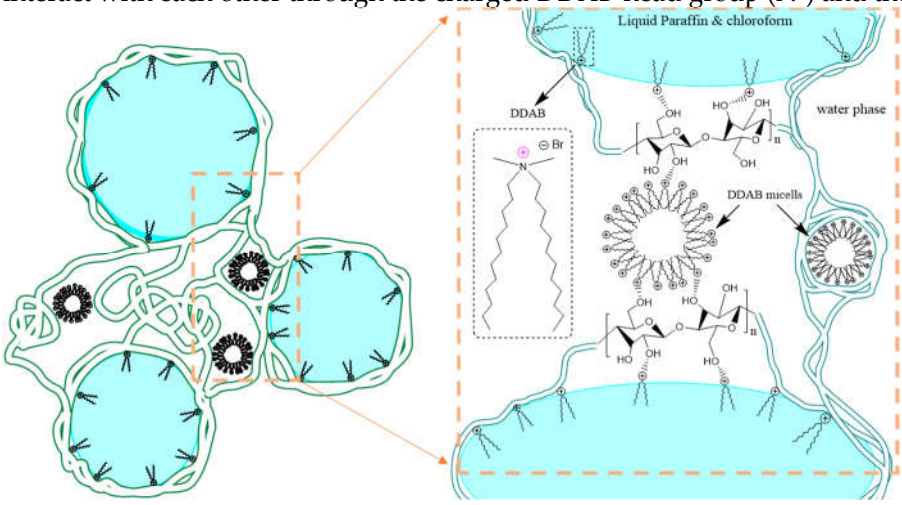

Figure 1. Schematic representations of CNF emulsion droplets, including the three CNF-crosslinked droplets attaching with DDAB monomer and micells, and the detailed interfacial structure that hydrogen bonding interaction forms aggregation among 3 kinds of molecules.

Preprints (www.preprints.org) | NOT PEER-REVIEWED | Posted: 12 October 2022 doi:10.20944/preprints202210.0170.v1

3.1.1. Polarized optical microscopy

Figure 2(a-h) show the optical microscopy images of several CNF emulsions with CNF content of 1%, 1.5%, 2% and 2.5% and DDAB content of either 0.1% or 0.5%. The droplets are generally round and exhibit a homogeneous size with diameters between 20 - 50 m, demonstrating the high stability of the interfacial films broad about by the CNFs. For the sample series with 0.1% DDAB content, the droplet size is more homogenously and smaller with increasing CNF content (Figure 2j). For the 0.5% DDAB content series, however, the droplet size is larger and relatively constant but lacks size homogeneity, which becomes obvious from the larger error bars. The error bars are caused by some droplets in the 0.5% DDAB content series being significantly larger than the others. Furthermore, they are also less spherical due to their large size and decreased surface tension. Moreover, a regional giant dark shadow can be noticed in any DDAB0.5% samples, which is indicative for dense accumulation of flexible CNF chains distributing at aqueous phase. However, the limitation of POM images is that it is not possible to visualize CNF-gathering in the aqueous phase further.

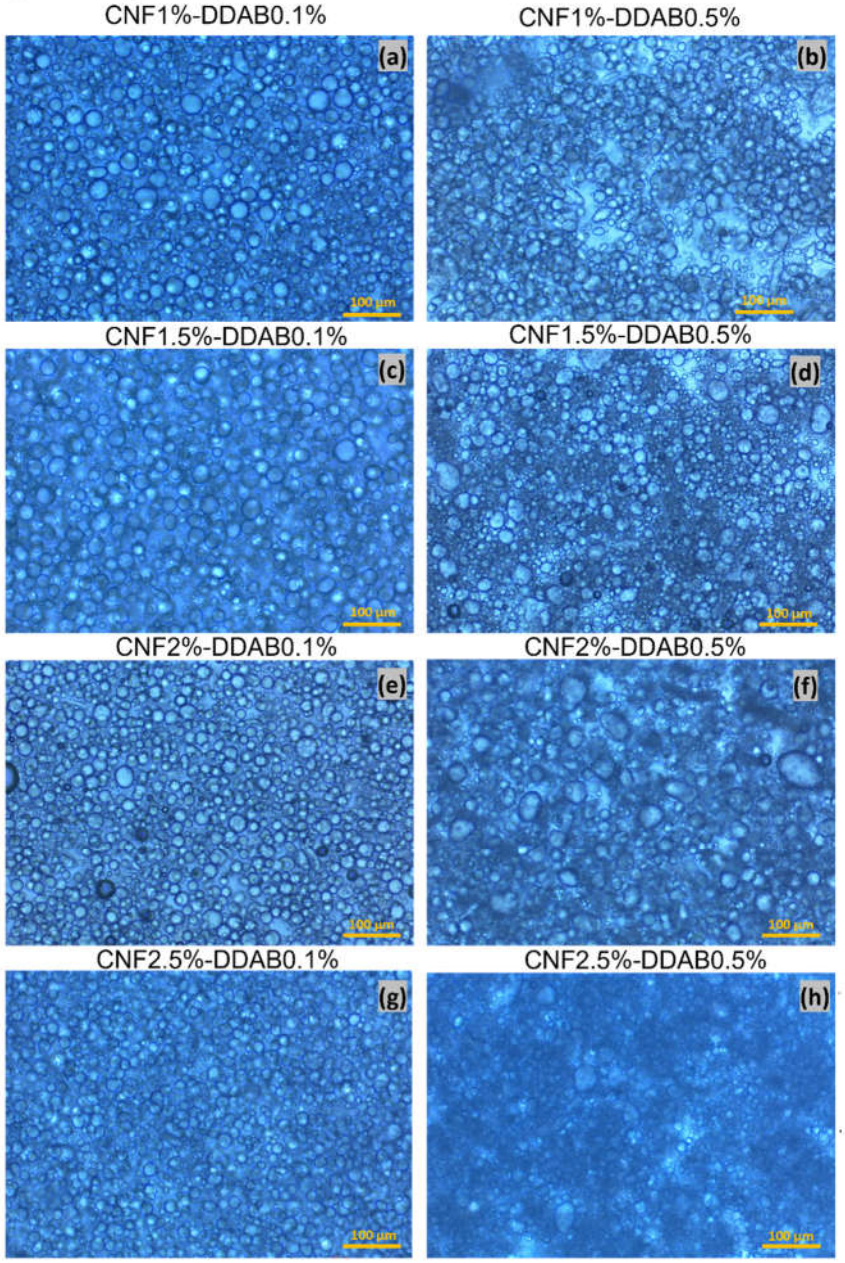

Preprints (www.preprints.org) | NOT PEER-REVIEWED | Posted: 12 October 2022 doi:10.20944/preprints202210.0170.v1

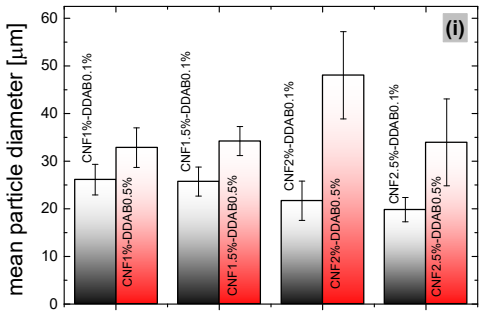

Figure 2. Optical microscopy characterization of (a-b) CNF1%-DDAB0.1&0.5%, (c-d) CNF1.5%-DDAB0.1&0.5%, (e-f) CNF2%-DDAB0.1&0.5%, and (g-h) CNF2.5%-DDAB0.1&0.5%. Contrast adjusted for improved visibility. (i) Column graph concerning the droplets' mean size. Sizes were determined by Image J.

3.1.2. Fluorescence analysis on CNF distribution

The vision of dense CNF accumulations was investigated by confocal laser scanning microscope with an excitation wavelength of 355 nm and a receiving wavelength of 430 nm. Figure 3(b-c) shows the fluorescent CNF have obvious green area distributing in the aqueous phase, while spherical droplets do not show the green spot because of no fluorescence appearing in such wave. When the DDAB content increases, the green light region, which represents the CNF distribution, expands merely in the aqueous phase and then covers partial droplets' view, which directly indicates that CNF emulsions become thicker and harder to flow. Consequently, CNF chains in the aqueous phase can bridge several oil droplets and form small micelles (without oil droplets inside), as shown in Figure 3(a). However, when the DDAB content increases, the CNF chains tends to separate against entanglement by itself, resulting in a stronger charged connection using DDAB micelles and smaller CNF flocs. These networks are displayed in the third draft in Figure 3(a) and contribute to higher viscosity and harder flowability, which affects the yield stress and would be proved in rheological studies.

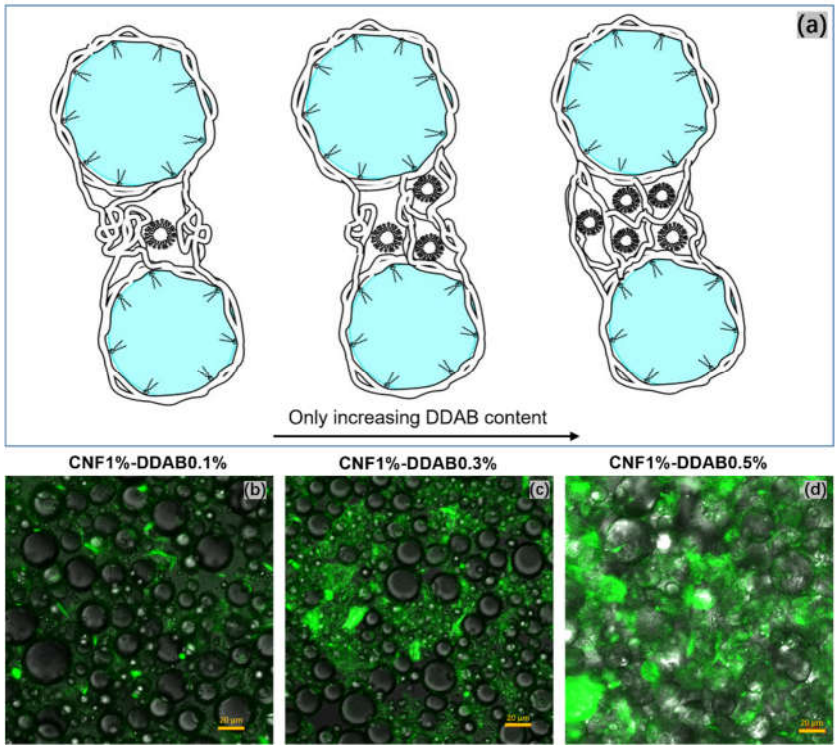

Figure 2. (a) Schematic representations of CNF distribution in aqueous phase with increasing DDAB micelles contents. Confocal laser scanning microscopic images of CNF emulsion with 1 wt.% CNF

 doi:10.20944/preprints202210.0170.v1

and (b) 0.1, (c) 0.3, and (d) 0.5 (wt.%) DDAB content after being stained with Calcofluor white, which shows the obvious difference of light shadow aggregation.

3.1.3. SEM analysis on CNF droplets

SEM images of 6 such dried CNF emulsions with three different CNF contents and two different DDAB contents are shown in Figure 3 (a-f). The roundest particles are found for CNF1.5%-DDAB0.1% (Figure 3b), indicating a stable interface, while CNF1%-DDAB0.1% and CNF1%-DDAB0.5% to a lesser degree show partially disintegrated droplets (Figure 3a, d). Higher CNF- and DDAB contents lead to inward dented surfaces of the droplets, which resemble soccer balls with too little pressure in them (Figure 3c, e, f). This can be explained by the fact that DDAB was introduced into the oil phase in chloroform solution; thus, up to 10% of the oil phases' volume is lost during the drying process, which leads to these deformed spheres if the interface is strong enough to resist shrinking.

When focusing on the chains on the droplets' surfaces of CNF2%-DDAB0.5%, the CNF networks can be clearly seen as well as bridging to neighboring droplets (Figure 4f), which is also observed at CNF1%-DDAB1% (white dashed wireframe, Figure 4g). Corresponding to (Figure 3b-d) and (Figure 4f, g), some CNF chains can maintain their appearance after drying and exist on the "ball" surface. Figure 4i shows these features for CNF1%-DDAB0.1% along with the EDS-images (Figure 4j (C), Figure 4k(O)), showing a homogeneous distribution of both atoms on the droplet. While paraffin, DDAB, and CNF obviously contain carbon, oxygen is only a minor fraction in paraffin and DDAB (theoretically 0). However, CNF contains carbon and oxygen in a 6:5 atomic ratio (the repeat unit of cellulose is $C_{12}H_{20}O_{10}$). Further, traces of water are possibly present in the sample as well. Thus, the determined amount of 5.1 wt.% oxygen (Figure. 4k) suggests coverage of the droplet with CNF but does not prove it because of the aforementioned alternative explanations. However, the theoretical oxygen content of CNF is much higher, so EDS mapping has to be a combination of CNF, DDAB, and paraffin signals.

The emulsion of CNF1%-DDAB0.1% has smaller particle sizes owing to the rather low CNF content being unable to stabilize larger droplets. The obvious shrinkage of the CNF-shell around the droplets due to drying (and thus the evaporation of the chloroform) leads to a relatively flat collapsed structure, unlike, e.g., CNF2%-DDAB0.1%, suggesting that the droplets' coverage with CNF is relatively thin, which therefore is not very stable against shrinkage of the droplet below the surface. For higher CNF contents, such as CNF2%-DDAB0.5%, the thicker CNF shell can not only stabilize larger droplets sufficiently but also extend to connect with other droplets.

Preprints (www.preprints.org) | NOT PEER-REVIEWED | Posted: 12 October 2022 doi:10.20944/preprints202210.0170.v1

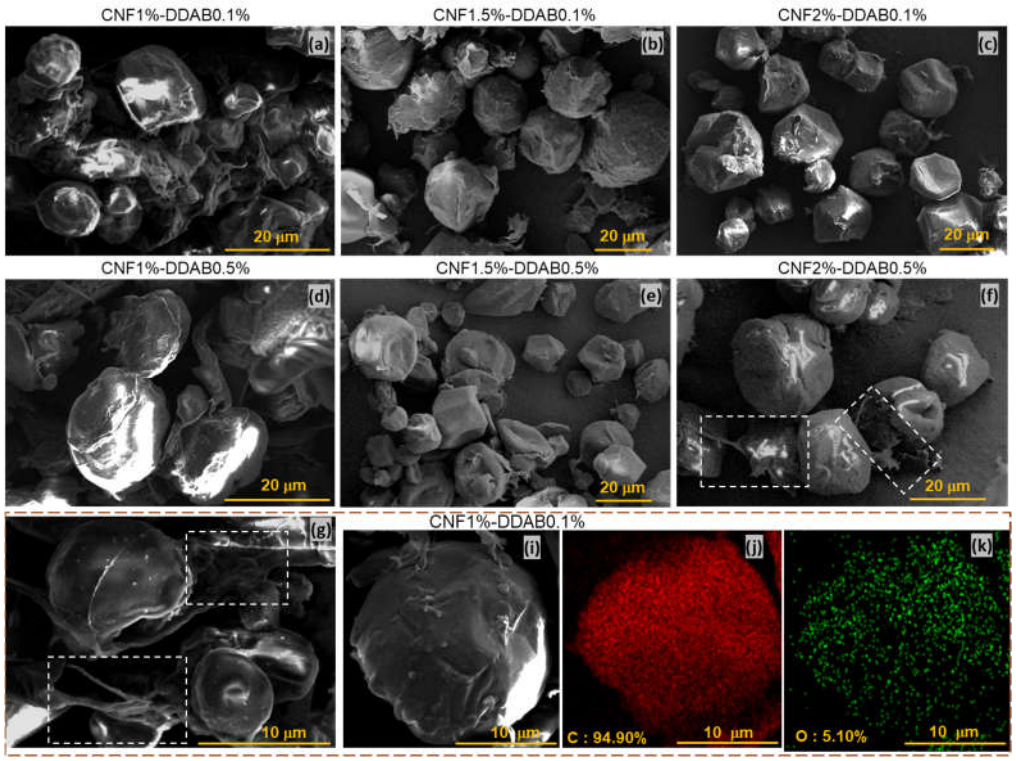

Figure 3. SEM images of CNF emulsions droplets for CNF contents in (a) 1%, (b) 1.5% and (c) 2% at 0.1 wt.% DDAB content and in (d) 1%, (e) 1.5% and (f) 2% at 0.5 wt.% DDAB content. SEM images for higher resolution of (g) and (i) CNF1%-DDAB0.1% and the EDS of elemental content and distribution of (j) carbon and (k) oxygen for one droplet.

3.2. Dielectric Spectroscopy

When an AC electric field stimulates the CNF emulsion, the charged and polarizable groups of CNF chains and DDAB will show a characteristic response, which allows extracting information on the emulsion properties. The parameters: σ^*, ε^*, z^*, δ_{min}, and $|\varphi|$, in this text were discussed importantly, that correspond to complex conductivity, permittivity, impedance, and the lowest shift factor calculated from the real and imaginary part of permittivity and phase angle of AC current and voltage, respectively. Their relevant functions were illustrated in the supplementary information of this work.

Figure 5(a-c) show that ε' and ε'' are plotted as a function of f after combining the data of the last loop for all CNF emulsion, which the equation of $\varepsilon'(f)$ and $\varepsilon''(f)$ obey the Debye's classical equations, expressed in Eq SI7 [46, 51]. There are obviously found of the similar characteristics for emulsion with different CNF- or DDAB- content and increasing ε' and ε'' in lower f, which indicates the strong polarization dependance on f owing to $\varepsilon'(\omega)\sim P$ according to Eq(SI6) [47]. More importantly, the curves of $\varepsilon'(f)$ and $\varepsilon''(f)$ are divided into two parts at $f = 10^3$ Hz, where $f < 10^3$ shows the deviation curves associating with lower slope of ε' but $f > 10^3$ shows a nearly overlapped of them, indicating the different relaxation domain [32]. In order to directly analyze the two domain, phase angle δ as a function of f for all emulsion are plotted in Figure 5(d-f) according to Eq(SI7) and Eq(SI8)), which shows very high damping (δ close to 90°) in most of the frequency range except for a minimum in the middle of the frequency range. The minimum of $\delta(f)$ of all CNF emulsions is located around $f = 10^3\sim10^4$ Hz and both sample series (0.1 and 0.5 wt.% DDAB) display a decrease in the δ-minimum (δ_{min}) with increasing CNF content. In contrast, emulsion stabilized with GO particles show the different behavior associating with δ_{min} (Figure SI5). $\delta > 45°$, corresponding to $\varepsilon' < \varepsilon''$, means that more energy is dissipated than stored. This explains the stronger heat loss during the dielectric test, because the testing samples are carbonized gradually (Figure SI7). CNF emulsion with lower CNF content displays remarkably hysteresis owing to the

Preprints (www.preprints.org) | NOT PEER-REVIEWED | Posted: 12 October 2022 doi:10.20944/preprints202210.0170.v1

higher δ and the decreasing charged content [48]. The content of the oxygen-containing functional group mainly affects the electric properties of CNF emulsion [49]. Moreover, increasing DDAB content at the interface can promote the adsorption between CNF and oil droplets, leading to a slightly decreasing loss angle (Figure 5g). Moreover, due to the obvious phase separation for CNF0.5%-DDAB0.5% before loading this sample, the behavior can be visualized and conclude the strong sensitivity of monitoring phase change by the dielectric characteristics.

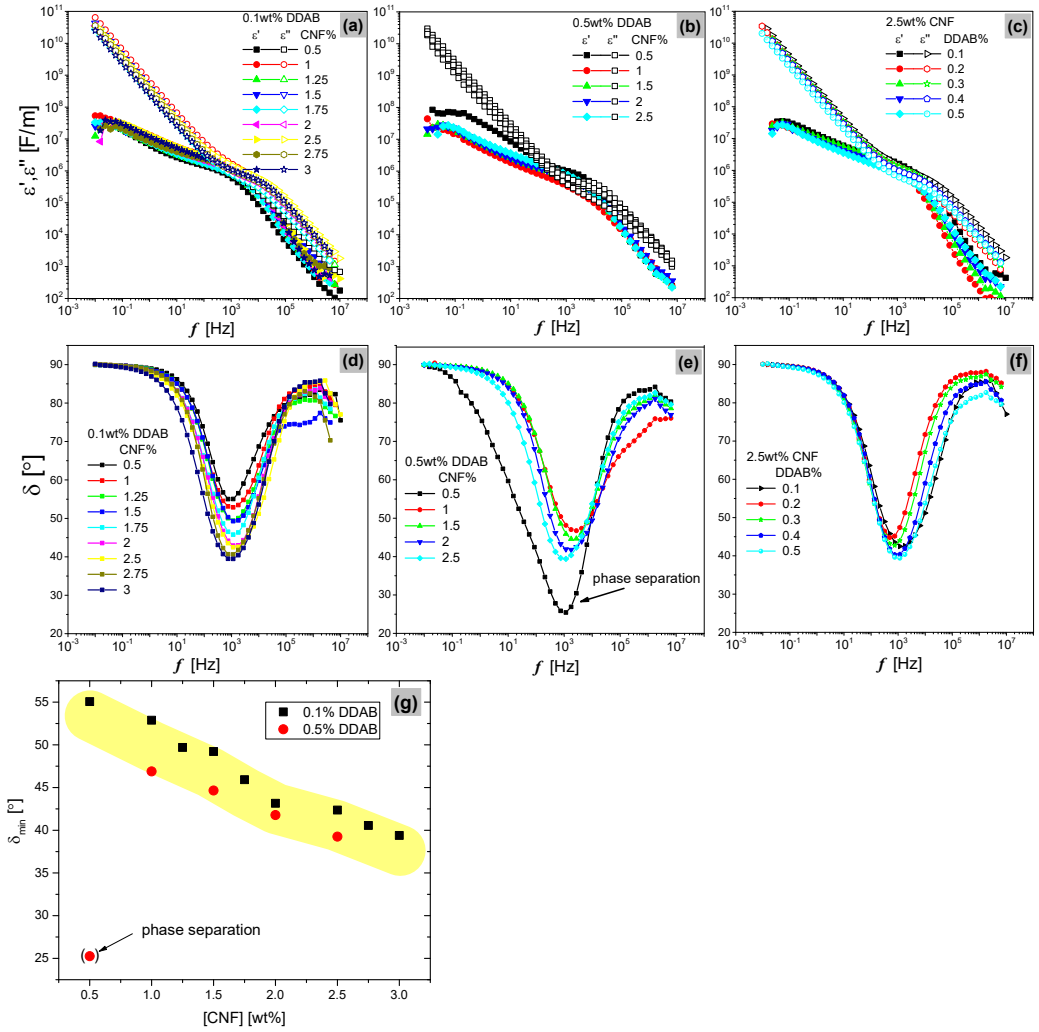

Figure 4. Graphs of permittivity and loss angle versus frequency for at different CNF or DDAB-content, such as (a, c) of CNFx%-DDAB0.1%, (b, e) of CNFx%-DDAB0.5% DDAB and (c, f) of CNF2.5%-DDABx%, respectively. (g) δ_{min} as a function of CNF-content and the phase separated sample show an obvious unfitting.

The characteristic data of $|\sigma^*|$, $|\varepsilon^*|$, and $|z^*|$ are listed in Table 2 based on the increasing trends of CNF or DDAB content. Here, loss angle has an opposite effect on the phase angle provided by the AC voltage and current, which means that less heat loss of CNF emulsion causes an increasing phase difference of AC voltage and current. When increasing DDAB content, the values of $|\sigma^*|$ and $|\varepsilon^*|$ behave the decrease trends but δ_{min} and $|\varphi|$ increase oppositely, as expressed in Eq(SI4 & SI5) [34, 50]. However, the absolute values of complex impedance stay relatively constant but for some unstable emulsion systems, such as CNF0.5%-DDAB0.1% & 0.5%. That their impedances are higher than others can obtain a method to characterize the stability of CNF emulsion by the large impedance. In addition, $|z^*|$ is proportional to $|\sigma^*|$ defined in Eq(SI2 and SI3)

Consequently, The CNF and DDAB concentration-dependent dielectric properties of CNF emulsion were investigated at 25°C in the frequency range of 10^{-2} to 10^{7} Hz. At $f = 10^{3}\sim10^{4}$ Hz, the minimum values corresponding to the electrode polarization relaxation

Preprints (www.preprints.org) | NOT PEER-REVIEWED | Posted: 12 October 2022 doi:10.20944/preprints202210.0170.v1

frequency strongly depend on increasing the CNF content but a slight influence by DDAB content. The complex permittivity of larger CNF content increase δ_{min} because of the more stimulation of ionic transfer in the AC field and polarization when introducing more CNF chains. However, the polarization process would be limited because of the more efficient connection between CNF and droplets at high DDAB content.

Table 2. Values of minimum loss angle during the whole frequency range and corresponding $|\varphi|$, $|\sigma^*|$, $|\varepsilon^*|$ and $|z^*|$ at same state dependence on different CNF or DDAB content.

CNF (wt.%)	DDAB (wt.%)	δ_{min} (°)	f (Hz)	$\lvert\varphi\rvert$ (°)	$\lvert\varepsilon^*\rvert \bullet 10^6$ (F/m)	$\lvert\sigma^*\rvert \bullet 10^{-3}$ (S/m)	$\lvert z^*\rvert$ (Ohm)
0.5		55.01	916.6	34.99	1.29	0.54	7.21
1		52.87	1175.92	37.13	1.99	1.28	2.05
1.25		49.39	1188.99	40.61	1.20	0.77	3.32
1.5		49.27	1379.02	40.72	1.29	0.82	3.85
1.75	0.1	45.76	1203.48	44.24	1.08	1.07	2.21
2		42.91	1430.01	47.09	1.36	0.87	3.65
2.5		42.47	1412.81	47.53	2.16	0.90	3.54
2.75		40.66	1063.07	49.39	1.80	0.75	4.23
3		39.46	1099.05	50.54	1.94	0.81	3.93
0.5	0.5	25.44	1078.02	64.56	1.10	0.70	6.28
1		46.74	2596.59	43.26	0.32	0.49	5.30
1.5		44.59	2204.97	45.41	0.71	0.70	2.96
2		41.77	1552.12	48.23	0.72	0.71	3.94
2.5		39.40	994.74	50.60	0.96	0.62	3.97
2.5	0.1	42.47	1175.92	47.53	2.16	0.90	2.29
	0.2	44.82	494.67	45.18	2.39	0.65	4.91
	0.3	42.72	764.70	47.28	2.18	0.91	3.65
	0.4	40.28	770.09	49.72	1.72	0.72	2.71
	0.5	39.40	1159.51	50.60	0.96	0.62	3.38

3.3. Rheology

3.3.1. Deformation-induced morphology changes

The arrangement of droplets before and after deformation can be investigated by fluorescence microscopy because of the paraffin's strong fluorescence at a wavelength λ = 460 nm and ideal depth of field (Figure 5). Comparing the droplets' sizes of the sample CNF2.5%-DDAB0.1% before deformation with the end of high shear rate, the droplets maintain the shape scale and size, however, the assembled feature of bulk droplets have a tendency to close to each other, then the larger space of aqueous phase is formed (Figure 5a). Kalashnikova et al. [16] have proved that the longer CNC nanocrystals would prepare the more aggregated droplets clusters, in other words, create entangled systems to interconnective droplets. Nomena et al. [51] illustrated that un-adsorbed soluble biopolymers can create a viscoelastic network for preventing droplets from creaming and then contribute to attractive depletion interaction. Moreover, the stronger CNF networks contribute to the elastic deformation of emulgel and its entanglement cannot destroy totally after high deformation in aqueous phase [41, 52]. Therefore, the residual recovery force is responsible for formation of droplets clusters.

Preprints (www.preprints.org) | NOT PEER-REVIEWED | Posted: 12 October 2022 doi:10.20944/preprints202210.0170.v1

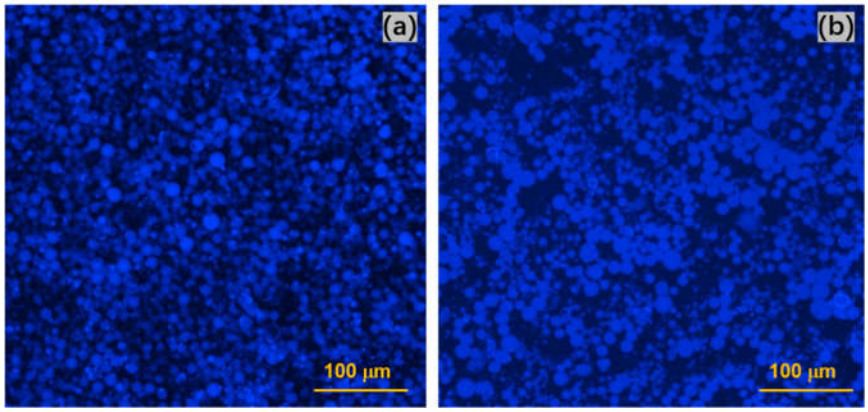

Figure 5. Fluorescence images of CNF2.5%-DDAB0.1% at (a) previous and (b) after deformation at a wavelength $\lambda = 460\ nm$ that was captured by the constant shear from 0.1 s^{-1} to 1000 s^{-1}.

3.3.2. Startup flows

For the multiple shear ramp profiles, 4 shear ramps (runs) were performed (run 1: $\dot{\gamma}$=0.01 s^{-1} → 1000 s^{-1}, run 2: $\dot{\gamma}$=1000 s^{-1} →0.01 s^{-1}, run 3: $\dot{\gamma}$=0.01 s^{-1} → 1000 s^{-1}, run 4: $\dot{\gamma}$=1000 s^{-1} →0.01 s^{-1}, no intermissions between them), which lasted 920 s each. None of the samples showed a clear normal force increase or decrease beyond ±0.3 N upon shearing (except for startup effects). The higher viscosity samples showed a slight decrease of normal force at $\dot{\gamma}$ >100 s^{-1} (Figure 6).[1] The first (and sometimes the second) startup flow ramp is always significantly higher than the following, almost identical in most cases (Figure 6). Thus, only the last segment - run 4 - is used for further evaluation.

The normal forces (open symbols) show a sharp decrease for $\dot{\gamma}$ below 0.1 s^{-1} in the first run, usually followed by a minor further decrease, which is due to the initial yield structure being broken up by the shear. More importantly, a decrease in the normal force is observed at $\dot{\gamma}$ >100 s^{-1}, which is typical of shear-thinning materials, except those with a plate or rod-like nanoparticles in them. This suggests that the effect of droplet deformation, which also decreases the normal force at high $\dot{\gamma}$ is less important than the influence of the CNF. The changes in normal force by ca. -0.1 N correspond to a first normal stress difference N_1 of ca. -51 *Pa*.

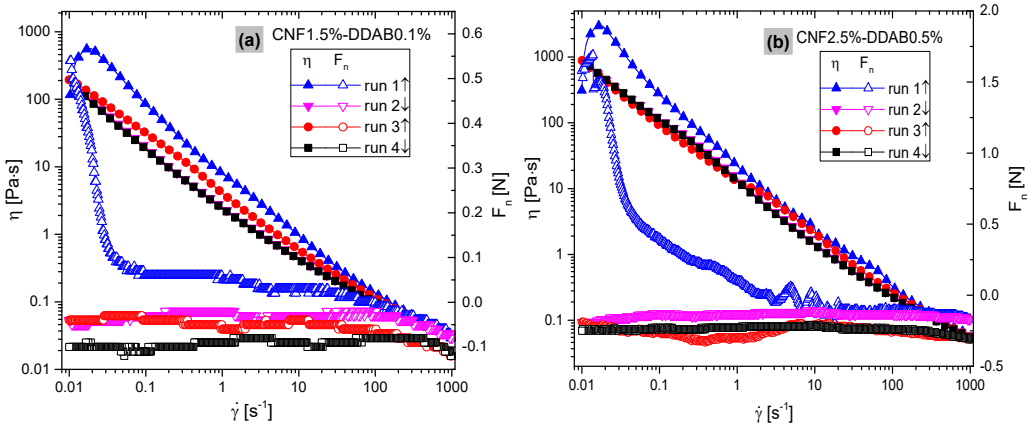

Figure 6. Viscosity (left axis) and normal force (right axis) as the function of shear rate at 1~4 ramps, showing the samples of (a) CNF1.5%-DDAB0.1% and (b) CNF2.5%-DDAB0.5%, respectively.

Figure 7 shows the results of the startup flows, determined by the multiple shear ramp profile and the startup flows of the miTT-test. For the multiple shear ramp, only the

[1] Please note that the normal force can only be measured with a precision of 0.01 N with the current setup – thus, its step-like appearance.

Preprints (www.preprints.org) | NOT PEER-REVIEWED | Posted: 12 October 2022 doi:10.20944/preprints202210.0170.v1

4th ramp ($\dot{\gamma}$ = 1000 s^{-1} → 0.01 s^{-1}) is shown in all cases. The SI shows some examples of the 1st-4th run (Figure SI7). The viscosity functions η($\dot{\gamma}$) of the samples with 0.1 wt.% DDAB (Figure 7a) appears relatively standard for a material with a yield point. Clearly, adding more cellulose (CNF) increases the viscosity, but at first glance, the shape of the viscosity functions is not significantly influenced by the changes in composition. A comparison between the multiple shear ramp and the miTT-startup flows shows a good agreement (±10%), demonstrating that both protocols deliver reliable values. When plotting the same data in terms of shear stress functions $\tau(\dot{\gamma})$ (Figure 7c), it becomes obvious that for the lowest shear rates $\dot{\gamma}$, τ approximately approaches a constant value, which can be understood as the yield stress τ_y, which increases with CNF-content (cf. Figure 8). However, when looking at $\tau(\dot{\gamma})$ for low shear rates in detail, it is obvious that the higher the CNF-content, the higher the shear rate $\dot{\gamma}$, at which a more or less constant value is reached and for the highest CNF-contents even a small increase towards the smallest $\dot{\gamma}$ is found, which indicate a structural recovery from the high shear rates imposed on the sample before.

When comparing the data of the samples with 0.5 wt.% DDAB (Figure 7b,d) with those with 0.1 wt.% DDAB (Figure 7a,c), the samples with 0.5 wt.% DDAB (except for the CNF0.5%-DDAB0.5%-O:W 1:2 sample, which is very similar to CNF0.5%-DDAB0.1%-O:W 1:2) show a clear kink between $\dot{\gamma}$ = 10 and 0.2 s^{-1}, which is visible for miTT-data as well. This clear difference suggests that the 0.5 wt.% DDAB has some structural changes that cause this unusual curve shape. This kink is even better visible as a step in $\tau(\dot{\gamma})$ (Figure 7d) and it is found for all 4 ramps in the experimental setup (Fig. SI5). For the same situation, Li et al. [17] and Jia et al. [53] found the similar steady-state viscosity curves and divided them to four regions: fibers' orientation, fibers' entanglement, networks' breakdown and well-oriented structure.

Considering this difference in rheological data when increasing the surfactant content fivefold (0.5 wt.% DDAB) and that it only happens when the CNF-content is sufficiently high (> 0.5 wt.%), it is clear that it has to be related to the stability of the interfaces, as those are strengthened by increasing surfactant (DDAB) and Pickering emulsifier/surfactant (CNF) content. Interestingly, the highest step is found for 1% (Figure 7d), while higher CNF-contents decrease the step significantly. The step could be interpreted as an increased viscosity due to a high shear-rate structure that collapses to a low resistance configuration once the shear rate $\dot{\gamma}$ is below this critical shear rate at the step (for CNF 1 wt.%, it is in the shear rate range 3-20 s^{-1}).

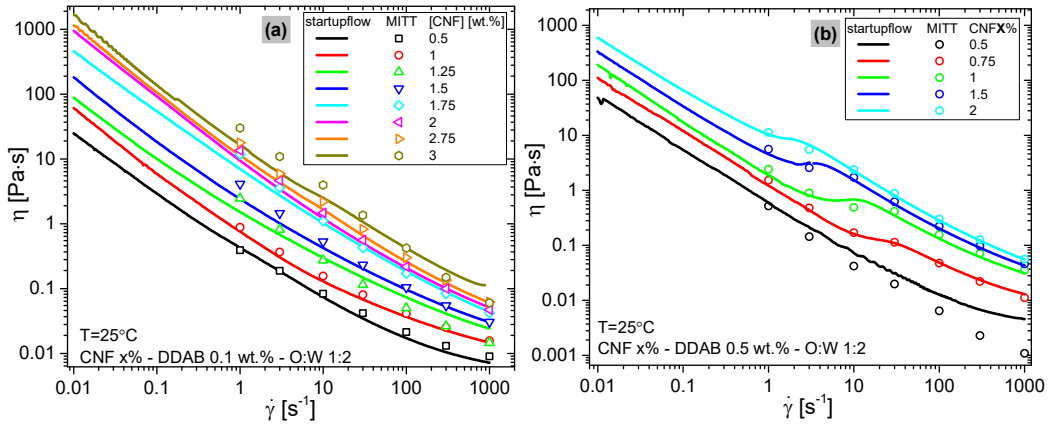

Preprints (www.preprints.org) | NOT PEER-REVIEWED | Posted: 12 October 2022 doi:10.20944/preprints202210.0170.v1

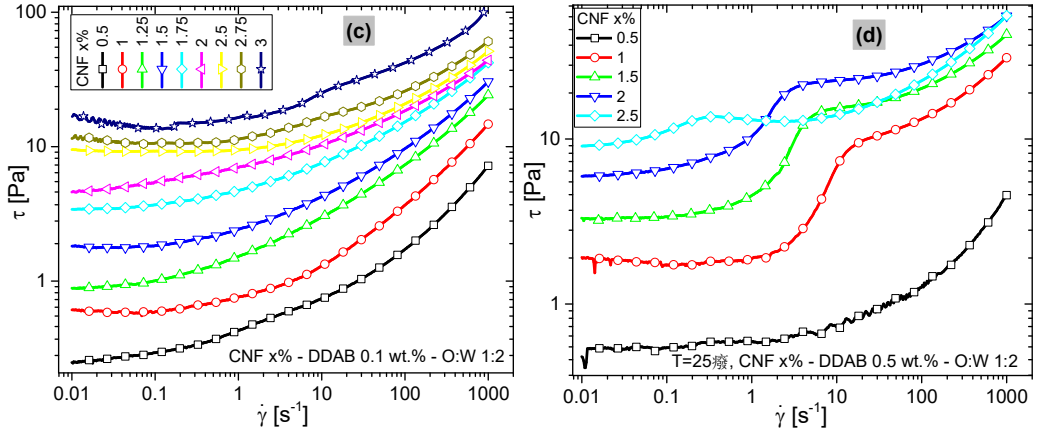

Figure 7. Startup flows in comparison with viscosity functions determined with the miTT protocol. Viscosity functions of (a) the 0.1 wt.% DDAB-series and (b) the 0.5 wt.% DDAB-series. Shear stress functions (c) the 0.1 wt.% DDAB-series and (d) the 0.5 wt.% DDAB-series.

In order to better compare the multitude of data, 2 characteristic quantities were defined: 1. The yield stress τ_y and 2. The maximum stress τ_{max} (at a shear rate $\dot{\gamma}$=1000 s^{-1}). The former was determined using a yield-stress modified Carreau-Yasuda model [54]:

$$\eta(\dot{\gamma}) = \eta_0(1 + (\dot{\gamma}/\dot{\gamma}_c)^a)^{\frac{n-1}{a}} + \tau_y/\dot{\gamma} \quad (1)$$

Where $\dot{\gamma}_c$ denotes the characteristic shear rate, a denotes the sharpness of the transition in a regular viscosity function, n denotes the slope of the viscosity function at a high shear rate (n=0 → dlogη/dlog$\dot{\gamma}$ = -1) and τ_y denotes the yield stress. As the contribution of τ_y dominates the viscosity function at low $\dot{\gamma}$, the other parameters were not evaluated, owing to their high dependence on each other. For the 0.5% DDAB sample series with the kink in the data, the fitted yield stress values τ_y were checked with extreme care and found within the range that one would determine manually from visually extrapolating the data towards $\dot{\gamma}$=0.

Figure 8a compares the yield stresses τ_y of both emulsion series as well as the maximum stress observed τ_{max} (at $\dot{\gamma}$=1000 s^{-1}). As already visible from Figure 7(c, d), an increase in the CNF-content leads to an increase of τ_y. Clearly, the differences between the 0.1 wt.% and the 0.5 wt.% DDAB is diminishingly small at high CNF contents, while they are more significant at low CNF contents. The maximum stress observed τ_{max}, which is always obvsered at the highest shear rate $\dot{\gamma}$=1000 s^{-1} shows a relation which appears to be similar to τ_y at a first glance, about 10 times the τ_y-value. However, when plotting the ratio τ_{max}/τ_y vs. CNF-content, it becomes clear that the higher the CNF-content, the lower is τ_{max}/τ_y and that it does not depend significantly on DDAB-content. For 0.5 wt.% CNF and 1 wt.% CNF, 0.1 wt.% DDAB (points in bracket), the relation does not show reliable values, which we attribute to the low yield stress τ_y, making a very precise determination difficult.

These findings can be explained by both CNF and DDAB stabilizing the interfaces. The emulsion consists of a water matrix with oil droplets that stabilize interfaces by DDAB and CNF. The yield stress τ_y is the resistance of the material against any flow, i.e., below τ_y the sample behaves as a solid. The yield point τ_y depends on how many the droplets are interlocked, i.e., how stiff their interfaces are. Very soft interfaces make it very easy for the droplets to slide past each other, while infinitely hard interfaces could theoretically lead to jamming [17, 55]. DDAB as a normal surfactant stabilizes the interface as a classical amphiphile, i.e., by sitting at the interface with the hydrophilic head in the aqueous phase and two hydrophobic tails in the oil phase. As a general rule, increasing the amount of amphiphile decreases the droplet size as coalescence is reduced due to the improved stabilization of the interface [16, 40, 56].

The relations in Figure 8 can be interpreted as the consequence of CNF stiffening the droplet surface, thus increasing the τ_y in an approximately exponential fashion, making

Preprints (www.preprints.org) | NOT PEER-REVIEWED | Posted: 12 October 2022 doi:10.20944/preprints202210.0170.v1

the yield stress well tailorable. The stress at $\dot{\gamma}$=1000 s^{-1} shows a similar relation but with a lower slope, so that the ratio τ_{max}/τ_y decreases with increasing CNF-content. This can be interpreted with the yield stress τ_y being stronger influenced by the stiffening of the interface than the behavior under strong shear. This can be explained by the structures hindering the flow being shear sensitive, i.e., they lose their strength upon applying a significant shear rate. Furthermore, the decreasing ratio τ_{max}/τ_y means that at high CNF-contents, jamming does not play a significant role as that would lead to an increasing τ_{max}/τ_y-ratio.

However, the situation needs to be considered from the point of view of the influence of CNF suspensions too. For this purpose, 2 wt.% CNF-suspensions (without an oil phase) were made with DDAB-contents of 0, 0.1, 0.3, and 0.5 wt.%, which will be discussed in the following sections. Those showed viscosity functions very similar to those shown in Figure 7 (see Figure. 10). The yield stresses τ_y are found to be 1 Pa for 0.1% DDAB and 3 Pa for 0.5% DDAB, which is lower than the τ_y values of 5 Pa and 6.5 Pa found for the CNF2%-0.1%DDAB-O:W 1:2 and CNF2%-0.5%DDAB-O:W 1:2 emulsions, respectively. When considering that the CNFs are mostly located in the aqueous phase of the emulsion, a comparison with the CNF1.25%-0.1%DDAB-O:W 1:2, CNF1.5%-0.1%DDAB-O:W 1:2, and CNF1.5%-0.5%DDAB-O:W 1:2 emulsions – having approximately the same concentration in the aqueous phase should be done too. For those samples yield stresses τ_y are found to be between 2 and 3 Pa, almost identical to the values found for the suspension. Thus, it is safe to conclude that the CNFs cause a major contribution to the yielding stress in suspension and the emulsion's oil-water interface-related processes.

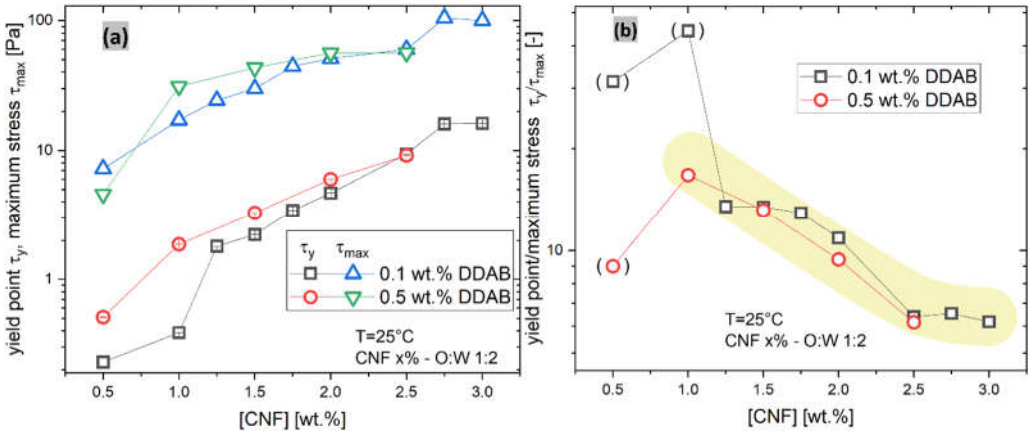

Figure 8. (a) dependence of yield stress values τ_y on the CNF or DDAB composition. The error bars are the uncertainties of the fit. (b) relation between viscosity at 10 s^{-1} and emulgel constituents.

In order to understand these results better, the non-emulsion equivalent of the emulsions was also tested – CNF-dispersions with variable DDAB-content. Figure 9(a-b) show the viscosity function of 2 wt.% CNF dispersion with 0, 0.1, 0.3 and 0.5 wt.% DDAB content. It is clearly visible that the data at high $\dot{\gamma}$ are almost undistinguishable, while at low $\dot{\gamma}$ a high DDAB-content leads to a quite significant yield stress τ_y of ca. 3 Pa (vs. ca. 6 Pa for CNF2% 0.5%DDAB O:W 1:2). At 0.1 wt.% DDAB content, only τ_y of ca. 1 Pa is found (vs. ca. 4.7 Pa for CNF2% 0.5%DDAB O:W 1:2). In comparison to the data for the Pickering emulsions, it is, therefore, clear that the yield stress τ_y varies significantly more and is lower. One might argue that CNF-content in the aqueous phase of the emulsion is higher than 2% and therefore, we have to compare the obtained yield stresses with those of emulsions with a lower CNF-content (e.g., based on O:W 1:2), an equivalent CNF-content should be reached around 1.3 wt. % CNF-content in the Pickering emulsions. However, such comparisons are difficult as it cannot be precisely accounted for how much of the CNF- and DDAB- is not in the aqueous phase in the Pickering emulsions. It is clear, however, that the dependence of the yield stress τ_y on the c is much larger for the CNF-dispersions (Figure. 8a) than for the Pickering emulgels, which suggests an equivalent

Preprints (www.preprints.org) | NOT PEER-REVIEWED | Posted: 12 October 2022 doi:10.20944/preprints202210.0170.v1

relation as plotted in Figure. 8b cannot be setup as no approximately DDAB-content independent τ_{max}/τ_y-ratio exists as can be also seen by comparing Figure. 7 and 9. Therefore, it is clear that the yield stress τ_y found for the Pickering emulsions is partially caused by the oil droplets and partially by the CNF-DDAB-agglomerates in the aqueous phase. Those CNF-DDAB-agglomerates are relatively weakly bonded, as can be seen from the fact that at high $\dot{\gamma}$, the viscosities are almost identical.

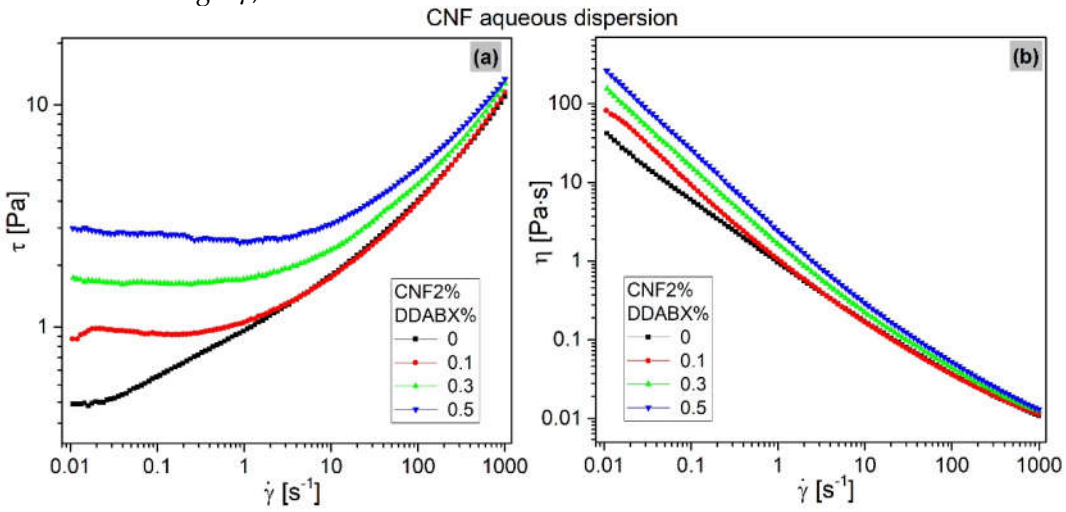

Figure 10. (a) stress function and (b) viscosity function of CNF water dispersion with 2 wt.% CNF-series.

4. Conclusions

A study of the properties of a Pickering emulsion with cellulose nanofibers (CNF) has shown that the behavior is determined by a combination of the properties of the regular surfactant DDAB in stabilizing the interfaces and of CNF stabilizing the interfaces as well as producing a colloidal network. The proper variation of the DDAB-content and CNF-content has helped in unraveling the interdependencies between these different components, which are very complex due to their interrelations.

The behavior of the Pickering emulsions is clearly determined by CNF and DDAB stabilizing the oil-water interface (proven by EDS), which solidifies the whole emulsion sufficiently to call it an emulsion. However, CNF is not only localized at the interface. It is also present in the form of more or less precipitated bridges and clusters in the aqueous phase, where it is stabilized by DDAB (micelles), too. The rheological properties show that most of the material properties can be explained by a combination of these 2 contributions. Microscopy has shown that the structure is mostly stable, although intensive shear has led to some minor modifications.

This paper has given a first overview of the properties of CNF Pickering emulsion. Part II will cover a much more in-depth rheological characterization that will lead to even deeper insights.

Supplementary Materials: Table SI1. The component ratio of aqueous phase including CNF gel weight and supplying water volume. Figure SI1. CNF emulsion pictures of (a) the mixture of oil-water before homogenization, (b) CNFX%-DDAB0.1% and (c) CNFX%-DDAB0.5%. Figure SI2. The appearance of CNF emulsion of (a) CNFX%-DDAB0.1% and (b) CNFX%-DDAB0.5%. Figure SI3. The actual photo and its sectional view of liquid cell that used to load CNF emulsion. Figure SI4. The dielectric raw data of 0.1wt% DDAB emulsion of (a, b) CNF1%, (c, d) CNF1.5%, (e, f) CNF2% and (g, h) CNF2.5% at all time intervals with the real and imaginary parts of permittivity and loss angle on dependence of dielectric frequency. Figure SI5. The dielectric raw data of 0.1wt% DDAB emulsion of (a, b) GO1% and (c, d) GO1.5% at all time intervals with the real and imaginary parts of permittivity and loss angle on dependence of dielectric frequency so as to compare the common properties of CNF emulsion. Figure SI6. The original data of startup-flow for 2 typical CNF emulgels. 1-4 ramps of shear rate were plotted with stress and normal force but the first ramp did

 doi:10.20944/preprints202210.0170.v1

not behave well because previous large deformations do not largely change the structure. Figure SI7. The pictures of (a) before and (b) after dielectric tests of CNF emulgel relating to carbonization.

Author Contributions: For research articles with several authors, a short paragraph specifying their individual contributions must be provided. The following statements should be used "Conceptualization, F.J.S, S.M.C. and G.M.Z.; methodology F.J.S. and S.M.C.; software, F.J.S..; validation, S.H.W., S.H. and Y.F.H.; formal analysis, S.M.C. and S.C.W.; investigation, S.M.C., W.Q.L.; resources, X.X.; data curation, F.J.S, S.M.C., S.H.W.; writing—original draft preparation, F.J.S, S.M.C.; writing—review and editing, F.J.S, S.M.C., Y.F.H. and G.M.Z; visualization, S.M.C., C.T.Z..; supervision, F.J.S, Y.F.H. and G.M.Z; project administration, F.J.S. and G.M.Z; funding acquisition, F.J.S. and G.M.Z. All authors have read and agreed to the published version of the manuscript." Please turn to the CRediT taxonomy for the term explanation. Authorship must be limited to those who have contributed substantially to the work reported.

Funding: : The authors are grateful to Shenzhen Fundamental Research Funds (Mianshang-Project JCYJ20210324093205013) and the National Natural Science Foundation of China (No. 51978410) for financial support.

Institutional Review Board Statement: Not applicable

Informed Consent Statement: Informed consent was obtained from all subjects involved in the study.
Data Availability Statement: the study did not report any data.

Acknowledgments: The authors are grateful to Shenzhen Fundamental Research Funds (Mianshang-Project JCYJ20210324093205013) and the National Natural Science Foundation of China (No. 51978410) for financial support.

Conflicts of Interest: The authors declare no conflict of interest.

References

1. Siqueira, G.; Kokkinis, D.; Libanori, R.; Hausmann, M. K.; Gladman, A. S.; Neels, A.; Tingaut, P.; Zimmermann, T.; Lewis, J. A.; Studart, A. R., Cellulose Nanocrystal Inks for 3D Printing of Textured Cellular Architectures. *Adv. Funct. Mater.* **2017,** *27* (12), 10.
2. Habibi, Y.; Lucia, L. A.; Rojas, O. J., Cellulose Nanocrystals: Chemistry, Self-Assembly, and Applications. *Chemical Reviews* **2010,** *110* (6), 3479-3500.
3. Bai, W.; Holbery, J.; Li, K., A technique for production of nanocrystalline cellulose with a narrow size distribution. *Cellulose* **2009,** *16* (3), 455-465.
4. Rampinelli, G.; Di Landro, L.; Fujii, T., Characterization of Biomaterials based on Microfibrillated Cellulose with Different Modifications. *Journal of Reinforced Plastics and Composites* **2009,** *29* (12), 1793-1803.
5. Syverud, K.; Stenius, P., Strength and barrier properties of MFC films. *Cellulose* **2008,** *16* (1), 75-85.
6. Iwatake, A.; Nogi, M.; Yano, H., Cellulose nanofiber-reinforced polylactic acid. *Composites Science and Technology* **2008,** *68* (9), 2103-2106.
7. Wang, J.; Tavakoli, J.; Tang, Y., Bacterial cellulose production, properties and applications with different culture methods - A review. *Carbohydr Polym* **2019,** *219*, 63-76.
8. Halib, N.; Ahmad, I.; Grassi, M.; Grassi, G., The remarkable three-dimensional network structure of bacterial cellulose for tissue engineering applications. *Int J Pharm* **2019,** *566*, 631-640.
9. Picheth, G. F.; Pirich, C. L.; Sierakowski, M. R.; Woehl, M. A.; Sakakibara, C. N.; de Souza, C. F.; Martin, A. A.; da Silva, R.; de Freitas, R. A., Bacterial cellulose in biomedical applications: A review. *Int J Biol Macromol* **2017,** *104* (Pt A), 97-106.
10. Mohammadkazemi, F.; Azin, M.; Ashori, A., Production of bacterial cellulose using different carbon sources and culture media. *Carbohydr Polym* **2015,** *117*, 518-523.
11. Li, Q.; Wang, Y. X.; Wu, Y. H.; He, K. H.; Li, Y.; Luo, X. G.; Li, B.; Wang, C. T.; Liu, S. L., Flexible cellulose nanofibrils as novel pickering stabilizers: The emulsifying property and packing behavior. *Food Hydrocolloids* **2019,** *88*, 180-189.
12. Capron, I.; Cathala, B., Surfactant-free high internal phase emulsions stabilized by cellulose nanocrystals. *Biomacromolecules* **2013,** *14* (2), 291-6.
13. Liu, X.; Shi, S.; Li, Y.; Forth, J.; Wang, D.; Russell, T. P., Liquid Tubule Formation and Stabilization Using Cellulose Nanocrystal Surfactants. *Angew Chem Int Ed Engl* **2017,** *56* (41), 12594-12598.
14. Salas, C.; Nypelö, T.; Rodriguez-Abreu, C.; Carrillo, C.; Rojas, O. J., Nanocellulose properties and applications in colloids and interfaces. *Current Opinion in Colloid & Interface Science* **2014,** *19* (5), 383-396.
15. Jiang, Y.; Liu, L. L.; Wang, B. J.; Sui, X. F.; Zhong, Y.; Zhang, L. P.; Mao, Z. P.; Xu, H., Cellulose-rich oleogels prepared with an emulsion-templated approach. *Food Hydrocolloids* **2018,** *77*, 460-464.
16. Kalashnikova, I.; Bizot, H.; Bertoncini, P.; Cathala, B.; Capron, I., Cellulosic nanorods of various aspect ratios for oil in water Pickering emulsions. *Soft Matter* **2013,** *9* (3), 952-959.

17. Li, M.-C.; Wu, Q.; Song, K.; Lee, S.; Qing, Y.; Wu, Y., Cellulose Nanoparticles: Structure–Morphology–Rheology Relationships. *ACS Sustainable Chemistry & Engineering* **2015,** *3* (5), 821-832.
18. Nomena, E. M.; van der Vaart, M.; Voudouris, P.; Velikov, K. P., Rheology of oil-in-water emulsions stabilised by native cellulose microfibrils in primary plant cells dispersions. *Food Structure* **2021,** *30*.
19. Zhang, Y.; Zhu, G.; Dong, B.; Wang, F.; Tang, J.; Stadler, F. J.; Yang, G.; Hong, S.; Xing, F., Interfacial jamming reinforced Pickering emulgel for arbitrary architected nanocomposite with connected nanomaterial matrix. *Nature communications* **2021,** *12* (1), 111.
20. Binks, B. P., Particles as surfactants - similarities and differences. *Current Opinion in Colloid & Interface Science* **2002,** *7* (1-2), 21-41.
21. Hong, J. S.; Ruhs, P. A.; Fischer, P., Localization of clay particles at the oil-water interface in the presence of surfactants. *Rheologica Acta* **2015,** *54* (8), 725-734.
22. Gelot, A.; Friesen, W.; Hamza, H. A., EMULSIFICATION OF OIL AND WATER IN THE PRESENCE OF FINELY DIVIDED SOLIDS AND SURFACE-ACTIVE AGENTS. *Colloids and Surfaces* **1984,** *12* (3-4), 271-303.
23. Binks, B. P.; Lumsdon, S. O., Effects of oil type and aqueous phase composition on oil-water mixtures containing particles of intermediate hydrophobicity. *Physical Chemistry Chemical Physics* **2000,** *2* (13), 2959-2967.
24. Hong, J. S.; Fischer, P., Bulk and interfacial rheology of emulsions stabilized with clay particles. *Colloids and Surfaces a-Physicochemical and Engineering Aspects* **2016,** *508*, 316-326.
25. Whitby, C. P.; Fornasiero, D.; Ralston, J., Effect of oil soluble surfactant in emulsions stabilised by clay particles. *J Colloid Interface Sci* **2008,** *323* (2), 410-9.
26. Shahidi, S.; Koch, C. R.; Bhattacharjee, S.; Sadrzadeh, M., Dielectric behavior of oil–water emulsions during phase separation probed by electrical impedance spectroscopy. *Sensors and Actuators B: Chemical* **2017,** *243*, 460-464.
27. Jiang, Q.; Sun, N.; Kumar, P.; Li, Q.; Liu, B.; Li, A.; Wang, W.; Gao, Z., Real-Time Analysis of the Stability of Oil-In-Water Pickering Emulsion by Electrochemical Impedance Spectroscopy. *Molecules* **2020,** *25* (12).
28. de Oliveira, H. P.; de Melo, C. P., Use of electrical impedance spectroscopy as a practical method of investigating the formation of aggregates in aqueous solutions of dyes and surfactants. *J Phys Chem B* **2011,** *115* (21), 6903-8.
29. Ghasemi, S.; Darestani, M. T.; Abdollahi, Z.; Hawkett, B. S.; Comes, V. G., Electrical impedance spectroscopy for determining critical micelle concentration of ionic emulsifiers. *Colloids and Surfaces a-Physicochemical and Engineering Aspects* **2014,** *441*, 195-203.
30. Klein, R. J.; Zhang, S.; Dou, S.; Jones, B. H.; Colby, R. H.; Runt, J., Modeling electrode polarization in dielectric spectroscopy: Ion mobility and mobile ion concentration of single-ion polymer electrolytes. *J Chem Phys* **2006,** *124* (14), 144903.
31. Sjöblom, J.; Skodvin, T.; Jakobsen, T.; Dukhin, S. S., Dielectric Spectroscopy and Emulsions. A Theoretical and Experimental Approach. *Journal of Dispersion Science and Technology* **1994,** *15* (4), 401-421.
32. Sen, S.; Boyd, R. H., Dielectric relaxation in amorphous linear aliphatic copolyesters. *European Polymer Journal* **2008,** *44* (10), 3280-3287.
33. Boyle, M. H., THE ELECTRICAL-PROPERTIES OF HETEROGENEOUS MIXTURES CONTAINING AN ORIENTED SPHEROIDAL DISPERSED PHASE. *Colloid and Polymer Science* **1985,** *263* (1), 51-57.
34. Hill, R. M.; Cooper, J., CHARACTERIZATION OF WATER-IN-OIL EMULSIONS BY MEANS OF DIELECTRIC-SPECTROSCOPY. *Journal of Materials Science* **1992,** *27* (17), 4818-4827.
35. Skodvin, T.; Sjoblom, J., Models for the dielectric properties of flocculated w/o-emulsions. *Journal of Colloid and Interface Science* **1996,** *182* (1), 190-198.
36. Gorbacheva, S. N.; Ilyin, S. O., Morphology and Rheology of Heavy Crude Oil/Water Emulsions Stabilized by Microfibrillated Cellulose. *Energy & Fuels* **2021,** *35* (8), 6527-6540.
37. Chen, J. H.; Liu, J. G.; Su, Y. Q.; Xu, Z. H.; Li, M. C.; Ying, R. F.; Wu, J. Q., Preparation and properties of microfibrillated cellulose with different carboxyethyl content. *Carbohydr Polym* **2019,** *206*, 616-624.
38. Ougiya, H.; Watanabe, K.; Morinaga, Y.; Yoshinaga, F., Emulsion-stabilizing effect of bacterial cellulose. *Biosci. Biotechnol. Biochem.* **1997,** *61* (9), 1541-1545.
39. Winuprasith, T.; Suphantharika, M., Properties and stability of oil-in-water emulsions stabilized by microfibrillated cellulose from mangosteen rind. *Food Hydrocolloids* **2015,** *43*, 690-699.
40. Kalashnikova, I.; Bizot, H.; Cathala, B.; Capron, I., New Pickering emulsions stabilized by bacterial cellulose nanocrystals. *Langmuir* **2011,** *27* (12), 7471-9.
41. Lu, Y.; Qian, X. L.; Xie, W. Y.; Zhang, W. T.; Huang, J.; Wu, D. F., Rheology of the sesame oil-in-water emulsions stabilized by cellulose nanofibers. *Food Hydrocolloids* **2019,** *94*, 114-127.
42. Costa, C.; Mira, I.; Benjamins, J.-W.; Lindman, B.; Edlund, H.; Norgren, M., Interfacial activity and emulsion stabilization of dissolved cellulose. *Journal of Molecular Liquids* **2019,** *292*.
43. Kim, J.-H.; Shim, B. S.; Kim, H. S.; Lee, Y.-J.; Min, S.-K.; Jang, D.; Abas, Z.; Kim, J., Review of nanocellulose for sustainable future materials. *International Journal of Precision Engineering and Manufacturing-Green Technology* **2015,** *2* (2), 197-213.
44. Dickinson, E., Hydrocolloids at interfaces and the influence on the properties of dispersed systems. *Food Hydrocolloids* **2003,** *17* (1), 25-39.
45. Zembyla, M.; Lazidis, A.; Murray, B. S.; Sarkar, A., Water-in-Oil Pickering Emulsions Stabilized by Synergistic Particle-Particle Interactions. *Langmuir* **2019,** *35* (40), 13078-13089.

46. Costa, A. L. R.; Gomes, A.; Cangussu, L. B.; Cunha, R. L.; de Oliveira, L. S.; Franca, A. S., Stabilization mechanisms of O/W emulsions by cellulose nanocrystals and sunflower protein. *Food Research International* **2022,** *152*.
47. Richert, R.; Wagner, H., The dielectric modulus: relaxation versus retardation. *Solid State Ionics* **1998,** *105* (1-4), 167-173.
48. Valentini, L.; Bittolo Bon, S.; Cardinali, M.; Fortunati, E.; Kenny, J. M., Cellulose nanocrystals thin films as gate dielectric for flexible organic field-effect transistors. *Materials Letters* **2014,** *126*, 55-58.
49. Niu, F.; Li, M.; Huang, Q.; Zhang, X.; Pan, W.; Yang, J.; Li, J., The characteristic and dispersion stability of nanocellulose produced by mixed acid hydrolysis and ultrasonic assistance. *Carbohydr Polym* **2017,** *165*, 197-204.
50. Skodvin, T.; Sjoblom, J.; Saeten, J. O.; Warnheim, T.; Gestblom, B., A TIME-DOMAIN DIELECTRIC-SPECTROSCOPY STUDY OF SOME MODEL EMULSIONS AND LIQUID MARGARINES. *Colloids and Surfaces a-Physicochemical and Engineering Aspects* **1994,** *83* (1), 75-82.
51. Nomena, E. M.; Remijn, C.; Rogier, F.; van der Vaart, M.; Voudouris, P.; Velikov, K. P., Unravelling the Mechanism of Stabilization and Microstructure of Oil-in-Water Emulsions by Native Cellulose Microfibrils in Primary Plant Cells Dispersions. *ACS Appl Bio Mater* **2018,** *1* (5), 1440-1447.
52. Chen, Y.; Xu, C.; Huang, J.; Wu, D.; Lv, Q., Rheological properties of nanocrystalline cellulose suspensions. *Carbohydr Polym* **2017,** *157*, 303-310.
53. Jia, X.; Chen, Y.; Shi, C.; Ye, Y.; Abid, M.; Jabbar, S.; Wang, P.; Zeng, X.; Wu, T., Rheological properties of an amorphous cellulose suspension. *Food Hydrocolloids* **2014,** *39*, 27-33.
54. Yasuda, K.; Armstrong, R. C.; Cohen, R. E., Shear flow properties of concentrated solutions of linear and star branched polystyrenes. *Rheologica Acta* **1981,** *20* (2), 163-178.
55. Li, M. C.; Wu, Q.; Moon, R. J.; Hubbe, M. A.; Bortner, M. J., Rheological Aspects of Cellulose Nanomaterials: Governing Factors and Emerging Applications. *Adv Mater* **2021,** *33* (21), e2006052.
56. Chanamai, R.; McClements, D. J., Dependence of creaming and rheology of monodisperse oil-in-water emulsions on droplet size and concentration. *Colloids and Surfaces a-Physicochemical and Engineering Aspects* **2000,** *172* (1-3), 79-86.